TECHNISCHE MECHANIK
an open access journal

journal homepage: www.ovgu.de/techmech

Tech. Mech., Vol. 39, Is. 3, (2019), 252–260

Received: 16.04.2019
Accepted: 31.07.2019
Available online: 01.10.2019

The effect of the skin-core structure of injection-molded isotactic polypropylene on the stress distribution in bending tests

R. Glüge[1⋆], N. Mahmood[3], I. Kolesov[2], H. Altenbach[1], M. Beiner[3,4], R. Androsch[2]

[1] Otto von Guericke University Magdeburg, Universitätsplatz 2, D-39106 Magdeburg, Germany
[2] Martin Luther University Halle-Wittenberg, Interdisciplinary Center for Transfer-oriented Research in Natural Sciences (IWE TFN), D-06099 Halle/S., Germany
[3] Martin Luther University Halle-Wittenberg, Faculty for Natural Science II, Institute for Chemistry, Heinrich-Damerow-Str. 4, D-06120 Halle/S., Germany
[4] Fraunhofer IMWS, Walter-Hülse-Str. 1, D-06120 Halle/S., Germany

Abstract: We examine the effect of the skin-core structure of isotactic polypropylene (iPP) in bending tests. The depth-dependent material properties are determined in tensile tests and mapped to a finite element model. This enables the examination of internal stresses during bending numerically. In a bending test, one usually expects a monotonic stress distribution across the thickness, provided that the material is homogeneous and does not strain-soften. We found that the structural gradient of injection-molded iPP easily overcompensates the monotonic stress dependence, such that the maximal equivalent von Mises stress lies well below the surface in the so called shear layer. The latter is a result of the injection molding process.

Keywords: polypropylene, bending, skin-core gradient, microtoming, elastic-plastic

1 Introduction

Polymer parts are usually produced by injection molding, where the polymer melt is injected into a cavity. Injection molding can produce both simple and intricate parts with high production output and high efficiency. During the process, the semicrystalline microstructure of the polymer forms under shear and thermal gradients, which cause variable morphologies between the skin and core of the molded sample. The resulting, often stratified microstructure affects the structural mechanical properties of the product. As a net result of the effects of shear, pressure, and thermal fields during injection molding, skin-core morphologies that exhibit a layer-like or gradient structure, where the orientation of macromolecules and crystals, the crystallinity and the crystalline-amorphous superstructure depend on the distance from the surface (Housmans et al. (2009); Katti and Schultz (1982); Russell and Beaumont (1980); Drummer and Meister (2014)).
Therefore, polymeric gradient materials are produced naturally upon injection molding, even when the cooling or the shear flow is not controlled explicitly. The skin-core microstructure was studied, e.g. in Fujiyama et al. (1988); Wen et al. (2004); Housmans et al. (2009); van der Meer (2003), among many others. Extended accounts to the structure formation in solidifying polymers and injection molding technology can be found in Kamal et al. (2009); Zheng et al. (2011). Here, the focus is on the mechanical skin layer effects in elasticity and at small plastic deformations.
A typical load case for thin-walled plastic components is bending, hence bending tests are commonly used to characterize polymer properties, see, e.g. Bledzki et al. (2015). In bending, stresses are usually highest at the surface, since the strains grow monotonically from the mid-plane. For the same reason, the mechanical properties of the surface affect the effective flexural properties disproportionately. Bending tests offer some advantages: Bending samples can neither neck (like in tensile tests) or buckle (like in compression tests), hence they are a versatile tool to characterize the mechanical properties beyond what can be obtained from uniaxial tests. However, unlike tensile tests, the structural properties (like force-displacement curves) cannot be mapped directly to material properties due to the inhomogeneous deformation. Only with simplifying assumptions, like material homogeneity and small strains, one can identify the material properties from measuring forces and displacements. Both presumptions are shaky for injection-molded iPP parts, which makes it difficult to obtain material parameters for materials with a depth-gradient in the material properties.
Furthermore, it raises questions regarding the stress distribution. One might expect the surface to be the most critical region for crack nucleation in bending, as it combines inhomogeneities (e.g. scratches) with the highest stresses. We were unable to find an examination of the stress distribution across the thickness which takes into account both the bending state and the material property gradient. We approach this gap by characterizing the material properties layer-wise and mapping the depth-dependent material data to a finite element (FE) model of a bending test. We find that the softer skin layer may well overcompensate this monotonic stress increase, leading the stress maximum approximately 0.5 mm to 0.7 mm *below* the surface in bending samples of 4 mm thickness. Near the surface, a drop of the equivalent von Mises stress of approximately 20 % is observed.

⋆ E-mail address: gluege@ovgu.de
doi: 10.24352/UB.OVGU-2019-023
2019 | All rights reserved.

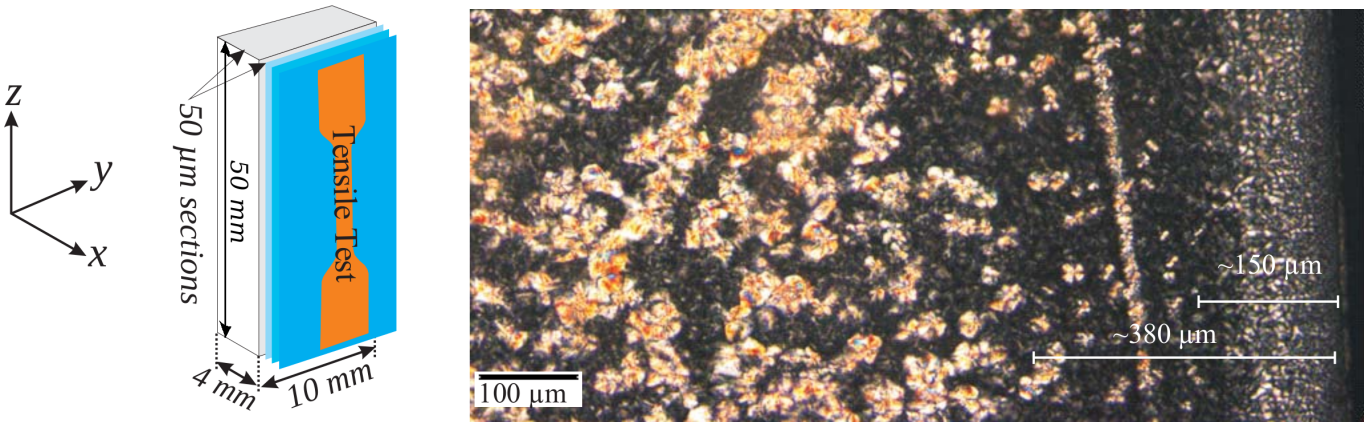

Figure 1: Left: Geometry of an injection-molded iPP sample for bending tests, the injection nozzle is at the center of the bottom plane. Right: micrograph inside the $x-z$-plane showing skin (right) and core (left) structure of a typical injection molded iPP sample.

2 Sample preparation and material characterization

2.1 Injection molding of the iPP samples

We manufactured bars of commercial iPP (Borealis HJ120UB) of dimensions 45 mm × 10 mm × 4 mm (see Fig. 1), using a BOY XS injection molding machine. The iPP was heated up to 200 °C. The mold temperature was 40 °C. The injection pressure was 350 bar. With these parameters, the filling time was about 1 to 2 seconds. After filling, a subsequent holding phase with a duration of 20 s and a holding pressure of 60 bar was applied. Subsequent cooling to room temperature under ambient pressure lastet about 4 minutes.

2.2 Skin-core structure

The micrograph in Fig. 1 gives an impression of the skin-core structure. It was examined thoroughly in a similar setup for different iPP materials and a sample width of 2 mm in Housmans et al. (2009). They distinguish four layers, namely the skin layer, the transition layer, the shear layer and the isotropic core. These layers have different main characteristics:

- The skin layer is cooled fastest, and has therefore the lowest crystallinity.
- The transition layer gets cooled down rapidly and sheared at the same time, which causes the polymer chains to orient collectively.
- The shear layer forms due to the interaction of the solidified skin layer and the flowing melt in the core during the injection. The shear layer has a higher crystal fraction, since it solidifies from the regular chain orientation from the transition layer. When the shear rate exceeds a critical value, the formation of crystal nuclei, as well as formation of β-crystals is observed.
- Regarding the isotropic core, the layers act as insulators, hence the core cools much slower without much shear flow, leading to an isotropic spherulitic structure.

The thickest layer is often the shear layer. Its thickness depends on the injection speed and ranges from 0.2 mm at high speeds to 1 mm at low speeds. It has a strong anisotropy and the highest β crystal fraction near the isotropic core (see Figs. 3, 4, 9 and 14 in Housmans et al. (2009)). Here, we join the very thin skin layer and the transition layer, which ranges from the surface to a depth of approximately 150 µm. The adjacent shear layer ranges to approximately 500 µm, where the isotropic core begins. These layer boundaries can be estimated by inspecting the polarized light image (Fig. 1). We also observed simultaneous changes of the depth-dependent material parameters at these depths. Nevertheless, since the transition is smooth, there is some vagueness in giving definite layer boundaries. We found that the fracture toughness that has been determined in tensile tests on thin slices is a good indicator, which shows a sudden drop between a depth of 400 µm and 500 µm. These results are collected in an upcoming article (Mahmood et al., N.D.).

2.3 Tensile testing of bulk specimen

The polymer block was clamped directly into a universal testing machine (Zwick/Roell Z010). The gauge length was assumed to be the clamping distance. The test speed was 27 mm/minute at a clamping distance of 27 mm, such that the nominal strain rate was $1/60\ \mathrm{s}^{-1} \approx 0.0176\mathrm{s}^{-1}$.

2.4 Tensile testing of thin films

The injection molded bars were cut in the y-z-plane into slices of 50 µm by stepwise microtoming from the surface to the core via a Leica SM2500E sectioning system. The toming direction was the z-direction. Tensile specimens (shouldered test bars) were punched out from these layers using a cutting-die unit according to ISO 527-2 Typ 5B. The positioning of the stencil was carefully adjusted to always cut out the shouldered test strip at the same position. The specimen size was $6 \times 35\ \mathrm{mm}^3$, with a specimen

gauge length of 12 mm. The tensile testing for the stress vs strain behavior was carried out on on a Zwick universal testing machine (Z010, Zwick/Roell) at room temperature and a testing speed of 12 mm/min. The testing speeds were adjusted in proportion to the gauge length, such that the nominal strain rate was the same ($1/60\ \mathrm{s}^{-1} \approx 0.0176\mathrm{s}^{-1}$) for all tests.
A total of 40 slices was examined, from a depth of 25 µm (mid-plane) to 1975 µm in steps of 50 µm. For each depth we averaged the results of at least 3 tests. For the largest sample set (7 slices) the standard deviation was less than 5% for Young's modulus. Some characteristic stress-strain curves are presented in Fig. 2 along with the fitted material model as detailed in the Sec. 2.5.

2.5 Material model

We did not examine the strain rate dependence in more detail. The material properties depend on the depth. We found the deformation plasticity theory using the Ramberg-Osgood-relationship (Ramberg and Osgood (1943)) to suit the stress-strain behaviour up to approximately 10 % of strain quite well at all depths, see Fig. 2 for some representative stress-strain curves. The Ramberg-Osgood-law gives the strains as an explicit function of the stresses

$$\varepsilon = \frac{1}{E}\left(\sigma + \frac{\sigma^n}{\sigma_\mathrm{y}^n}\right) \tag{1}$$

with three material parameters, where E is Young's modulus, σ_y the yield stress and n the hardening exponent. The Ramberg-Osgood-model does not introduce plastic strains but is a nonlinear elasticity which mimics an elastic-plastic behavior, similar to the deformation theory of plasticity by Hencky (1924) and Ilyushin (1947). Therefore, it cannot be applied if unloading or strain path changes occur.

Yield limit As can be seen in Fig. 2, a pronounced yield point is not visible. In such cases, the yield point is defined according to some rule, the well known 0.2 % residual strain rule is one example. For the Ramberg-Osgood law, the residual strain at σ_y is $1/E$. For our measurements of $E \approx 600$ MPa . . . 1200 MPa, this corresponds to a residual strain between $0.08\overline{3}$ % and $0.1\overline{6}$ %, i.e., a reasonable yield point definition.

Hardening Note that larger values of n imply less hardening, hence the inverse hardening exponent $1/n$ actually quantifies the hardening. $1/n$ is the slope of the stress-strain-curve beyond the yield point in a double logarithmic plot.

Fitting the parameters E, σ_y and n to the experimental data The three parameters were fitted by the least squares method to the experimental data in the strain interval from 0 to 10 %, which is just before necking occurs in most of the tests. This was done for all layers between 25 µm (mid-plane) and 1975 µm in steps of 50 µm. The adopted material parameters are plotted over the depth in Fig. 3. One can see that on the surface, stiffness, yield strength and hardening have a local minimum, which makes the surface the mechanically weakest part. Conversely, approximately 300 µm below the surface, Young's modulus and the inverse hardening exponent have a local maximum, while the yield stress remains roughly the same. At approximately 700 µm below the surface, Young's modulus has a local minimum, the yield stress a local maximum and the inverse hardening exponent drops to approximately 0.08. Since the core material is more brittle, there is an increased scattering of the results. In this depth range, the experimental data was replaced by a trend line, see Fig. 3.

3 Layer properties vs bulk properties

One may have noticed that the layer-wise stiffnesses and yield limits are somewhat lower than the bulk properties of iPP. Young's modulus lies usually between 1300 MPa and 1800 MPa, the yield stress lies mostly between 25 MPa and 35 MPa. Here, the average Young modulus of the layers is approximately 920 MPa, while the bulk's Young modulus is approximately 1320 MPa. Hence, the elastic properties are underestimated by a factor of approximately 0.7, see Fig. 2. At first glance, this is unexpected, since one might expect that the bulk Young modulus is close to the average of the layer-wise moduli. This systematic discrepancy is a result of the loss of scale separation. The layers exhibit, in proportion to the volume, a large surface with zero stresses, i.e. homogeneous stress boundary conditions. It is well known from homogenization theory that such samples underestimate the effective stiffness (see, e.g. Glüge et al. (2012)). Therefore, a fine discretization of the slices across the thickness is opposed by a loss of the scale separation. This is a fundamental dichotomy.
From a descriptive point of view, the layer's Young moduli are lower because of a lack of load distribution which is present in the bulk. Due to the inhomogeneity of the material, the local stresses deviate from the imposed uniaxial tensile state. Near the surface, the stresses confined to a plane stress state. This plays no big role in the bulk tensile tests, where the plane stress confinement makes up only a small portion. But in the layer-wise tests, the stresses are forced to be plane practically everywhere. This robs the slices of one dimension for the load distribution, as sketched in Fig. 4.
The loss of scale separation is larger in the core, since the core contains spherulites, the diameters of which are almost as large as the slice thickness of 50 µm (see Fig. 1). Near the surface, a finer microstructure prevails. This explains the increased scattering in the core Figs. 3.
Note that these observations apply to the effective elastic and plastic properties, although the effect appears less pronounced for the plasticity. For our fitting procedure, we found the bulk sample to have a yield limit of only 16 MPa, but in conjunction with an exceptionally high inverse hardening exponent of 0.18, such that the bulk is effectively stronger than most layers, see Fig. 2. Since for our bending tests the plastic properties are more relevant, we take the values as they were measured, keeping in mind that the overall stress levels, stiffness and strength of the bending sample are rather underestimated.

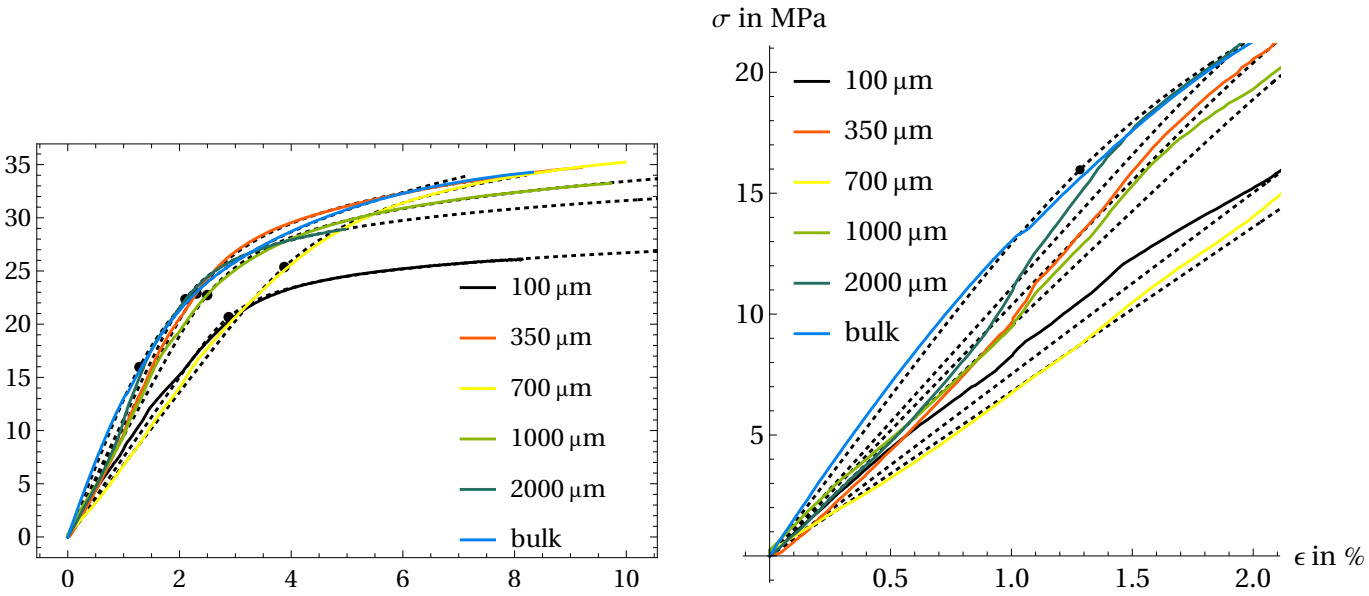

Figure 2: Left: True stress over engineering strain curves obtained on thin sections at different depths, where the number indicates the starting depth of the layer (e.g., ”100 µm” indicates the third layer, spanning the depth from 100 µm to 150 µm). The coloured solid lines correspond to the tensile test data, the black dotted lines represent the fitted material model (eq. 1). The black dots indicate the yield point as obtained from fitting the Ramberg-Osgood material parameters. The bulk stress strain curve shows a higher stiffness and strength than most layers. Only at a depth of 350 µm, the bulk stress is exceeded in a small interval. Right: Zoom on the elastic portion. The bulk's Young modulus is considerably larger than any of the Young moduli of the slices.

4 Bending tests

To examine the effect of the surface layer, bending tests were simulated numerically.

4.1 Test setup

The samples described in Sec. 2.1 were subjected to a three point bending test. Both bars ends jut out 10 % of the sample length of 45 mm, which leaves a load span of 36 mm. The loading head and the supporting points are freely rotating cylinders with a diameter of 8 mm. A sketch drawn to scale is given in Fig. 5.

4.2 Simulations

To examine the stress distribution, finite element (FE) simulations were devised.

4.2.1 Finite element setup

A finite element model of the bending test was created, for which we used the FE system Abaqus. We compared three different material property distributions, namely homogeneous core material (as found at a depth of 2 mm), homogeneous skin layer material (as found at the surface) and depth-dependent according to the material data as presented in Sec. 2.5. Due to the symmetry, only one half of the sample was modelled. The simple geometry of the sample calls for a structured mesh with hexahedral elements, with a mesh refinement near the surface and the contact points. An impression of the meshing is given in Fig. 6. To avoid shear locking, we used quadratic shape functions. The bending load head and the support points were modelled as rigid surfaces, since the steel barrels are much stiffer than the iPP. The barrels are in frictionless contact to account for the pivoted mounting. Since large deformations occur, a geometric nonlinear framework is used.

4.2.2 Simulation results

The most interesting result, namely the reduced surface stress due to the softer skin layer is depicted in Fig. 6 (FE model) and Figs. 8 to 9 (stress accross thickness).

Force displacement curves The force-displacement curves are depicted in Fig. 7. One can see that the pure skin material sample is much softer, compared to the pure core and the inhomogeneous samples. The latter do not differ significantly.

Stress distribution over depth The stress distribution is depicted along a line through the cross section in the center of the sample (see Fig. 6). One can see the typical compressive and tensile normal stresses as expected in a bending test in Fig. 8. It is also visible that the equivalent von Mises stress drops about 20 % near the surface, from approximately 30 MPa at a depth of

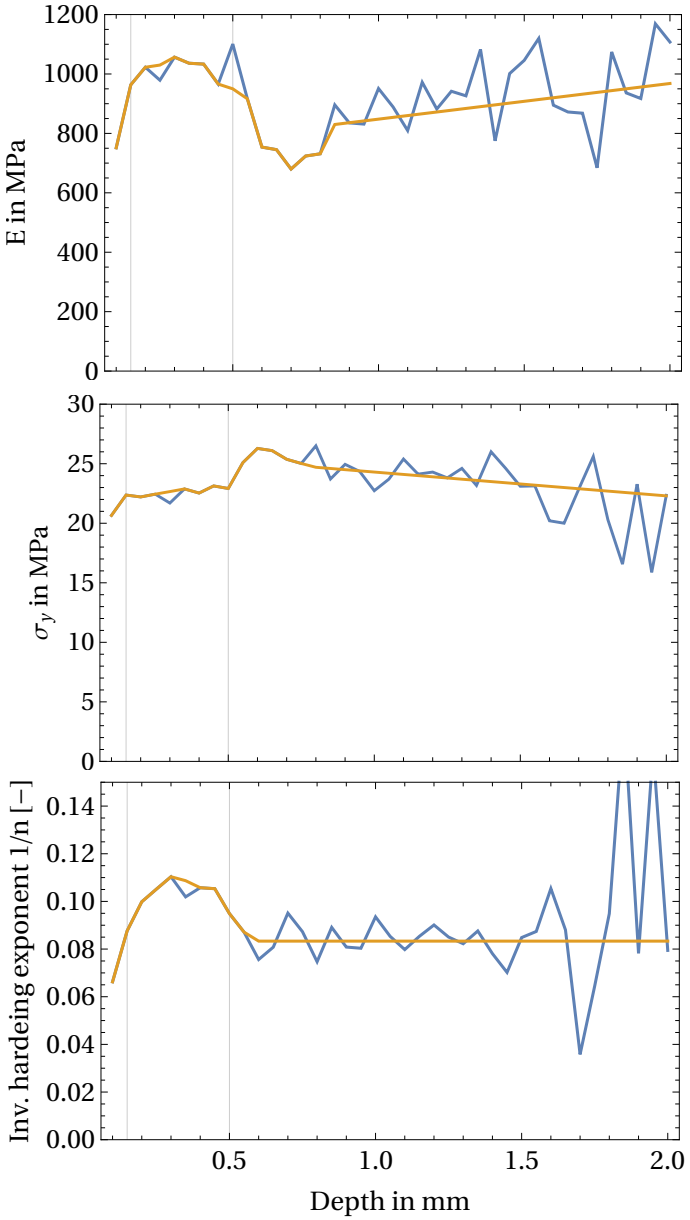

Figure 3: Young's modulus E, the yield stress σ_y and the inverse hardening exponent $1/n$ over the depth in mm as fitted to the tensile test data (blue) and after removal of the scattering via a trend line (yellow). One can see that stiffness, yield strength and hardening rate have a minimum at the surface. The vertical lines indicate the layer transitions.

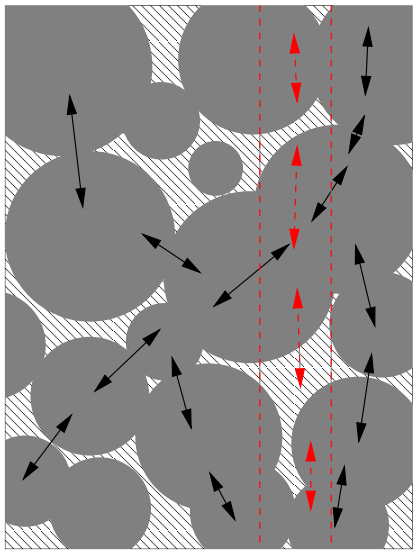

Figure 4: The semi-crystalline spherulites are much stiffer than the amorphous matrix. Under effective tension in the vertical direction, the load distribution runs mostly through adjacent spherulites. If the bulk is sliced, the load distribution is locally forced to run through the softer matrix, making the slices appear softer. Note that this is just a rough description of the load redistribution, it does not take into account more intricate effects that may take place at the phase boundaries.

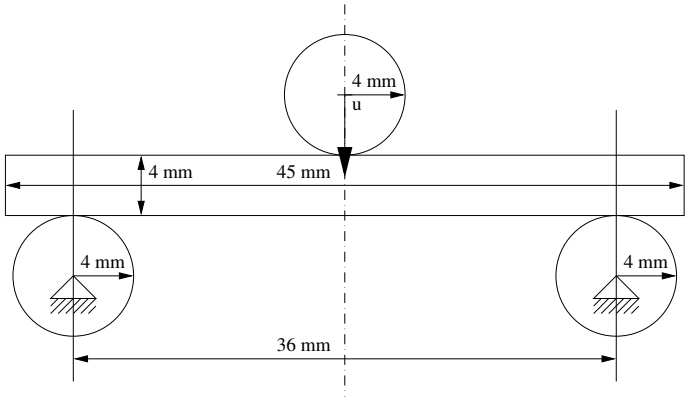

Figure 5: Bending setup drawn to scale.

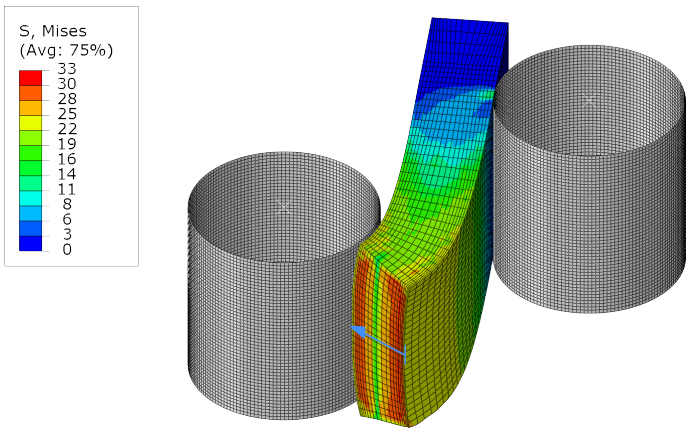

Figure 6: Equivalent von Mises stress distribution at a displacement of approximately 9 mm. One can see a considerable decrease of the equivalent von Mises stress in the skin layer. The stress distribution along the arrow is depicted in Fig. 9.

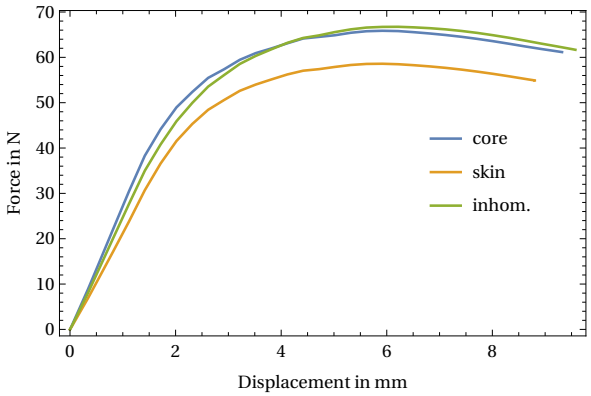

Figure 7: Force-displacement curves for the three cases (pure core material, pure skin material, inhomogeneous).

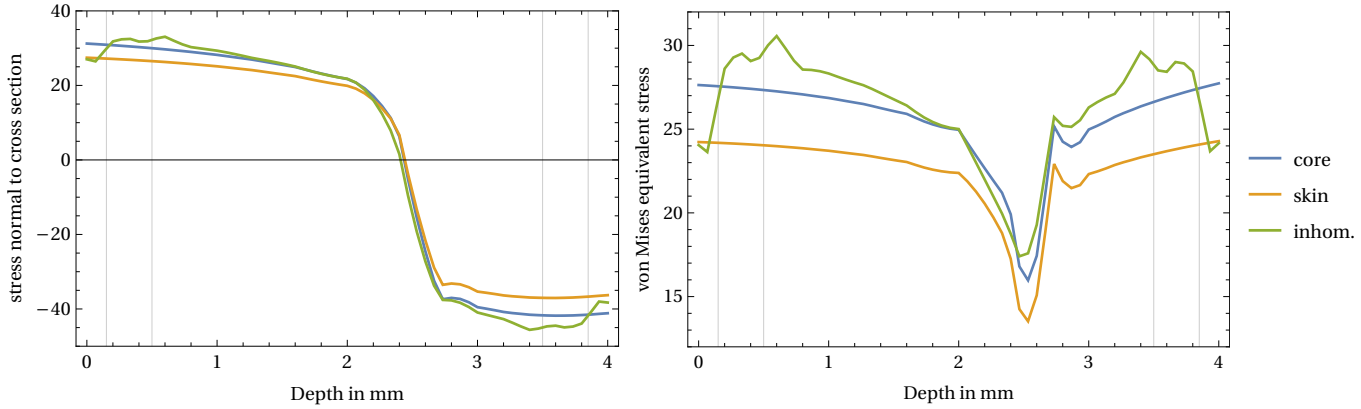

Figure 8: Left: Normal stress distribution through the bending sample near the bending load head for the three cases at the load maximum at a displacement u of approximately 9 mm. Note the slight shift of the neutral axis due to the large deflection and the compressive loading at the bending load head at a depth of 4 mm. The vertical lines indicate the layer boundaries between the skin- shear- and core layer. Right: Equivalent von Mises stress distributions for the three cases at different load head displacements. In the inhomogeneous case, a considerable stress drop near the surface is observed. The vertical lines indicate the layer boundaries between the skin- shear- and core layer.

approximately 500 µm to approximately 24 MPa at the surface. This effect is observed from the very beginning, but it is more pronounced the larger the strains become (see Fig. 9 top). This is in a sense counter-intuitive, as the outermost layers are subject to the largest strains in bending tests. We clearly see that the influence of the material property gradient is stronger than the approximately linear strain increase inside the cross section due to the bending.

5 Summary

We sliced a bulk iPP sample into layers of 50 µm thickness, the material properties of which were characterized in a tensile test. The material parameters were mapped to a finite element model of a bending test, of which the stress distribution across the thickness was analyzed. Our results can be summarized as follows:

- In the strain range up to 10 % and in the low strain rate limit, the tensile stress-strain behavior of iPP can be modeled well using the Ramberg-Osgood material law with only three parameters, namely Young's modulus, the yield stress and the inverse hardening exponent.
- Unfortunately, the layer-wise properties that were measured cannot be correlated directly with the bulk properties due to a loss of scale-separation. Either the discretization is coarse, or the layers are too thin to be representative. Specifically, the confinement to a plane stress state excludes a local load distribution mechanism in the microstructure, which makes the layers appear softer than the bulk. This affects the elastic properties, which are underestimated on average by a factor of approximately 0.7, more than the plastic properties.

  Since the spherulite size is larger in the core, the loss of scale separation is bigger in the core. This implies that the tensile tests underestimate the core stiffness more than the skin stiffness, which means that the unbiased material property gradient may be even stronger.
- The depth profile of these material parameters is rather complex, see Fig. 3. Going from the skin to the core, we find directly at the beginning of the skin/transition layer that all three parameters exhibit a local minimum ($E \approx 750$ MPa, $\sigma_y \approx 20$ MPa, $1/n \approx 0.06$), making the outermost layer softest and weakest. The adjacent shear layer from approximately 150 µm to ≈ 500 µm is stiffest and strongest, having a global maximum of Young's modulus of ≈ 1050 MPa and the inverse hardening exponent of ≈ 0.11 at a depth of ≈ 300 µm. In the shear zone, the yield stress increases monotonically. Near the start of

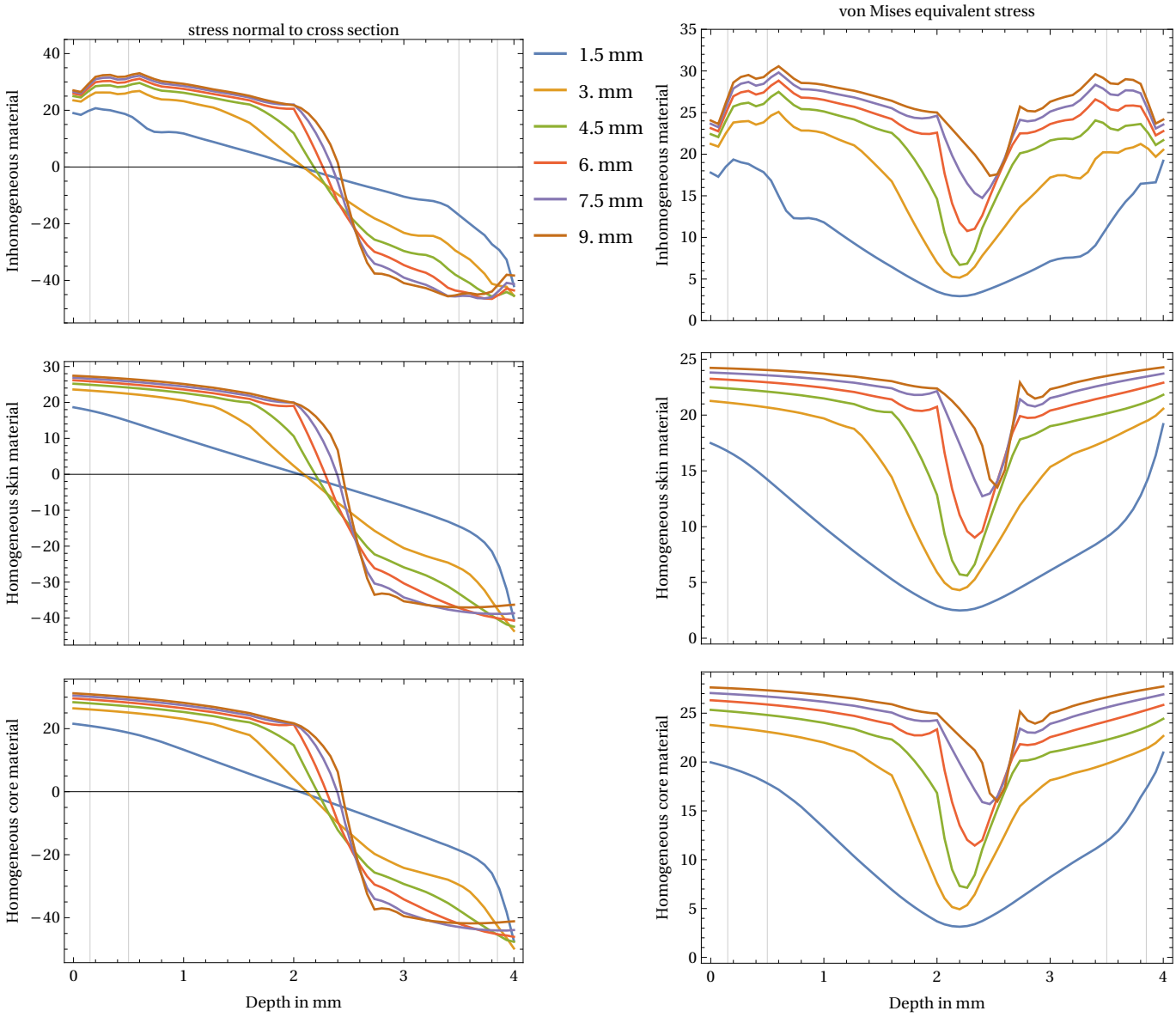

Figure 9: Left: Normal stress distribution (left column) and equivalent von Mises stress distribution (right column) through the bending sample near the bending load head at different load head displacements, shown for the inhomogeneous material (top row), the pure skin material (middle row). The vertical lines indicate the layer boundaries between the skin- shear- and core layer. Note the slight shift of the neutral axis due to the large deflection and the compressive loading at the bending load head at a depth of 4 mm. Most important, the upper right plot shows a significant drop of the equivalent von Mises stress near the skin.

the core, the yield stress has a global maximum of ≈ 26 MPa at ≈ 600 µm, while Young's modulus has a local minimum of ≈ 700 MPa at a depth of ≈ 0.7 µm, before a homogeneous property profile with average material parameters starts at ≈ 900 µm.

- The gradient of the material properties along the depth is rather strong. It easily overcompensates the linear strain-increase due to the bending deformation. Naturally, the effect is strongest after plastic deformations, where it can produce an equivalent von Mises stress drop from 30 MPa to 24 MPa in a depth from 0.5 mm to 0 mm, but it appears already in the elastic range. Young's modulus drops from ≈ 1000 MPa to ≈ 750 MPa at the surface over a thickness of only 0.1 mm. This is a strong gradient, which easily overcompensates the linear strain growth in the bending deformation.

References

A.K. Bledzki, P. Franciszczak, and A. Meljon. High performance hybrid pp and pla biocomposites reinforced with short man-made cellulose fibres and softwood flour. *Composites Part A: Applied Science and Manufacturing*, 74:132–139, 2015.

D. Drummer and S. Meister. Correlation of processing, inner structure, and part properties of injection moulded thin-wall parts on example of polyamide 66. *International Journal of Polymer Science*, 2014, 2014.

M. Fujiyama, T. Wakino, and Y. Kawasaki. Structure of skin layer in injection-molded polypropylene. *Journal of Applied Polymer Science*, 35(1):29–49, 1988.

R. Glüge, M. Weber, and A. Bertram. Comparison of spherical and cubical statistical volume elements with respect to convergence, anisotropy, and localization behavior. *Computational Material Science*, 63:91–104, 2012.

H. Hencky. Zur Theorie plastischer Deformationen und der hierdurch im Material hervorgerufenen Nachspannungen. *Zeitschrift für angewandte Mathematik und Mechanik*, 4:323–334, 1924.

J.-W. Housmans, M. Gahleitner, G.W.M. Peters, and H.E.H. Meijer. Structure-property relations in molded, nucleated isotactic polypropylene. *Polymer*, 50(10):2304–2319, 2009.

A. A. Ilyushin. Theory of plasticity at simple loading of the bodies exhibiting plastic hardening. *Rossíiskaya Akademiya Nauk (Prikl. Mat. Mekh.)*, 11:291, 1947.

M.R. Kamal, A.I. Isayev, and S.J. Liu. *Injection Molding: Technology and Fundamentals*. Polymer Processing Society, Progress in Polymer Processing. Hanser, 2009. ISBN 9783446416857.

S.S. Katti and M. Schultz. The microstructure of injection-molded semicrystalline polymers: A review. *Polymer Engineering & Science*, 22(16):1001–1017, 1982.

N. Mahmood, I. Kolesov, R. Glüge, H. Altenbach, R. Androsch, and M. Beiner. Influence of structure gradients in injection moldings of isotactic polypropylene on their mechanical properties. *Submitted for publication*, N.D.

W. Ramberg and W.R. Osgood. Description of stress-strain curves by three parameters. *Technical Note No. 902*, pages 1–28, 1943.

D.P. Russell and P.W.R. Beaumont. Structure and properties of injection-moulded nylon-6. *Journal of Materials Science*, 15(1): 197–207, Jan 1980.

D.W. van der Meer. Structure-property relationships in isotactic polypropylene, 6 2003.

Bianying Wen, Gang Wu, and Jian Yu. A flat polymeric gradient material: preparation, structure and property. *Polymer*, 45(10): 3359–3365, 2004.

R. Zheng, R.I. Tanner, and X.J. Fan. *Injection Molding: Integration of Theory and Modeling Methods*. Springer Berlin Heidelberg, 2011. ISBN 9783642212635.